Polymer 51 (2010) 6193–6202

Contents lists available at ScienceDirect

Polymer

journal homepage: www.elsevier.com/locate/polymer

Facile synthesis of melamine-based porous polymer networks and their application for removal of aqueous mercury ions

Guangwen Yang, Heyou Han*, Chunyan Du, Zhihui Luo, Yanjun Wang

College of Science, State Key Laboratory of Agricultural Microbiology, Huazhong Agricultural University, 1 Shizishan Street, Wuhan 430070, PR China

ARTICLE INFO

Article history:
Received 29 July 2010
Received in revised form
8 October 2010
Accepted 28 October 2010
Available online 2 November 2010

Keywords:
Melamine-based polymer
Schiff base chemistry
Mercury

ABSTRACT

Based on a facile catalyst-free process using Schiff base chemistry, here, highly cross-linked porous aminal networks in high yields (up to 90%) were rapidly prepared via microwave irradiation. The polymer networks contained as high as 50 wt% of nitrogen (N), in situ doped with sulfur (S), with specific surface areas of up to 301 $m^2\ g^{-1}$, and were also found to exhibit a solvent-based luminescence property. Adsorption kinetics and isotherm studies demonstrated that the Hg^{2+} removal by these polymers was extremely rapid (90% being attained within 5 min for a 400 mg L^{-1} Hg^{2+} solution) and highly efficient (up to 1172 mg g^{-1}). Particularly these materials also exhibited an excellent selectivity towards Hg^{2+} over other interfering ions (Cd^{2+}, Ni^{2+}, Zn^{2+}, Cu^{2+}, Co^{2+}, Ca^{2+}, Mn^{2+} and Mg^{2+}). Studies by FT-IR, Raman and XPS spectra showed that all the N-containing groups (triazine ring, primary amine, and secondary amine) as well as S-containing groups on the polymer matrix could be responsible for the Hg adsorption, through the mechanism of surface complexation.

1. Introduction

Porous organic polymers have been an appealing topic in the scientific community in recent years mainly due to their wide variety of applications such as gas storage, molecular separations, heterogeneous catalysis, pollutants adsorption, etc. [1–3] They are highly designable solid supports and the main potential advantage is the synthetic diversity [4,5]. General methods for their synthesis often rely on expensive, complex building blocks to be incorporated into these emerging materials and/or require the use of costly noble metal catalysts or strong Lewis acids catalysts [6]. Thus, the effective design and catalyst-free synthesis of new functional porous polymers from simple, cheap and readily available molecular monomer remains a challenging and important line of research in polymer chemistry [7]. Triazines, especially melamines, that can recognize other molecules by the donation and acceptance of hydrogen bonds, metal chelation, and π–π interactions, have proven their great potential in the rising areas of supramolecular [8] and dendrimer [9] chemistry. Melamine (MA), 66% N by mass, is a cheap and abundant triazine monomer used extensively in the plastic, medicinal, decorative, and paper industries. It is also a good candidate to be employed as raw material to prepare N-rich materials (i.e., carbon nitride and N enriched carbons) with weak basic functionalities [10,11], which have a broad spectrum of applications such as metal-free catalysis [12], adsorption of CO_2 [13], supercapacitors [11], and other industrial processes. Specially, the s-triazine ring with good stability and N functionality has recently become a remarkable unit in porous polymer fabrication. For example, studies on porous covalent triazine-based framework (CTF), which is an excellent catalyst support for metal particles exhibiting very high surface areas and high thermal and chemical stability, have gained considerable momentum [7,14,15]. Until now, however, the MA is seldom used as monomer to directly synthesize porous polymer without fussy templates.

More recently, Schwab et al. developed a new class of high-performance porous polymer networks, namely Schiff base networks (SNW), with high surface area by condensation of MA with several aromatic aldehydes through Schiff base chemistry in dimethyl sulfoxide (DMSO) [16]. Surprisingly, the structure of the polymer consists of aminal (–HN–C–NH–) networks instead of imine (–C=N–), and the proposed mechanism is that the imine double bond of the Schiff base subsequently attacked by primary amines ($-NH_2$), resulting exclusively in the generation of an aminal. As far as we are aware, Schiff base chemistry is a novel chemical approach in the synthesis of porous polymers, but the yield of the products, which is an important parameter for estimating the practical value of the method in potential applications, is only 61–66% with long reaction time (three days). Since the first report

* Corresponding author. Tel./fax: +86 27 87288246.
E-mail address: hyhan@mail.hzau.edu.cn (H. Han).

0032-3861/$ – see front matter © 2010 Elsevier Ltd. All rights reserved.
doi:10.1016/j.polymer.2010.10.052

in 1986, microwave irradiation that has advantages of energy saving, high conversion, and rapidity has been a very popular tool in organic and inorganic synthesis [17,18]. It is commonly used to quickly optimize reactions, boost speed and yield, and enhance product purities or material properties. DMSO, a typical dipolar aprotic organic solvent with a high dielectric constant and known to be microwave-friendly, can decompose relatively rapidly upon reflux under microwaves without the aid of catalysts, and the main decomposition products are sulfur derivatives, water and formaldehyde [19]. Thus, DMSO cannot only serve as a solvent, but also provide a source of S and reducing agent [20].

Pollution caused by anthropogenic contaminants has become a serious threat to the limited freshwater sources in the world. Hg, as one of the most toxic heavy metals commonly found in aquatic systems, can cause serious human disease, even at quite low concentrations [21]. Though there have been various techniques to treat Hg-contaminated waters, adsorption occupies a prominent place, in such a way that the Hg can be cheaply and easily removed [22]. Previous studies have shown that Hg ion tends to form stable chelates with N- and S-containing functional groups, such as $-NH_2$, $-NH-$, $-N=$, $-CN$, $-SR$, $-SH$, and so on [21,23]. Many effective Hg ion sorbents have been prepared by the immobilization of these groups onto the surface of various solid matrixes, including activated carbon [23,24], polymer [22,25–27], mesoporous silica [28], etc. Among all the materials, polymer sorbents have recently attracted more attention because of their larger adsorption capacity, higher efficiency and easier preparation [29]. Nevertheless, the development of new polymer sorbents for rapid, selective and effective removal of aqueous Hg ion still remains a great challenge for both industrial processing and environmental remediation.

Based on the above consideration, we rapidly synthesized a series of N-rich polymer networks in good yields, in situ doped with S (2–4 wt%), by a facile one-pot approach via microwave irradiation without any catalysts. The structures and properties of the resulting materials were systematically characterized by various important techniques. Additionally, for the first time, the potential applications of these polymer particles on the removal of Hg^{2+} have been investigated by static experiments and a possible adsorption mechanism is proposed.

2. Experimental

2.1. Materials

Terephthalaldeyde (TA, 98%) was purchased from TCI (Tokyo, Japan). MA (99.5%) was supplied from Tianjin Guangfu Fine Chemical Research Institute (Tianjin, China). All other reagents of analytical grade were purchased from Sinopharm Chemical Reagent Co. (Shanghai, China) and used without further purification unless otherwise noted. DMSO was dried and stored with molecular sieves (4 Å). All solutions were prepared with high-purity water (18.2 MΩ cm).

2.2. Synthesis of SNW

The SNW polymers were synthesized at a fixed overall molar concentration of 0.4 M and a constant volume of DMSO 20 ml. A typical procedure for preparation of SNW-D particles was as follows: MA (577 mg, 4.571 mmol), TA (460 mg, 3.429 mmol) and DMSO (20 ml) were added to a dried 50 ml three-necked round-bottom flask which was fitted with thermometer probe and mechanical stirrer. After degassing by dry N_2 bubbling and forming a clear solution, the mixture was heated to 180 °C for 4 h under microwave irradiation using a maximum power of 300 W. The resulting polymer precipitates were recovered by filtration and washed extensively with excess acetone, THF and CH_2Cl_2 to remove non-reacted reactants and the decomposition products of DMSO not bound to the networks. The solvent was removed under vacuum at room temperature to afford the polymers as off-white powders (see the Supporting Information).

2.3. Adsorption experiments

The adsorption of Hg^{2+} onto SNW polymers was performed in a batch experiment. It was carried out in a series of 50 ml glass bottles containing 50.0 mg of the SNW particles and 25.0 ml of $Hg(NO_3)_2$ aqueous solution whose Hg^{2+} concentration ranged from 1 to 60 mM. The bottles were sealed and shaken in an air bath (30 °C, 120 rpm). After shaking for a desired period, the solution was then filtered and the concentration of Hg^{2+} in the filtrate was analyzed by Volhard titration at higher Hg^{2+} concentration [21,30] or Cold vapor atomic absorption spectrometer (CV-AAS) analysis at lower Hg^{2+} concentration (less than 50 mg L^{-1}). The selectivity adsorption of the SNW for Hg^{2+} was similar to the above procedure, except the aqueous solution containing Hg^{2+} and other ions. After adsorption equilibrium, the concentration of Hg^{2+} in the remaining solution was measured by CV-AAS and various other ions concentration was simultaneously analyzed by Inductive Coupled Plasma Optical Emission Spectrometer (ICP-OES). The sample was diluted with distilled water when the absorbance exceeded the range of calibration curve. The adsorption capacity and the adsorptivity of the adsorbent were calculated according to the equations [21].

2.4. Measurements

The solubility of the SNW was evaluated by the method published by Li et al. [31] Elemental analyses were performed with a Perkin–Elmer 2400 Series II CHNS analyzer. UV/Vis adsorption spectra were acquired on a Nicolet Evolution 300 UV/Vis spectrometer. Fluorescence spectra were conducted on a Perkin–Elmer Model LS-55 luminescence spectrometer equipped with a 20 kW xenon discharge lamp as a light source. Scanning electron microscopy (SEM) images were taken by a JEOL JSM-6700F field emission scanning electron microscope. FT-IR spectra were collected on a Nicolet Avatar-330 spectrometer with 4 cm^{-1} resolution using the KBr pellet technique. Raman spectra were recorded by a Renishaw inVia Raman spectrometer equipped with a He–Ne laser excitation source operating at 633 nm. X-ray photoelectron spectra (XPS) were measured by a Thermo VG Multilab 2000 spectrometer equipped with a monochromatic Al Kα radiation source at room temperature. Thermal gravimetric analysis (TGA) measurements were examined using a NETZSH TG 209C thermobalance from room temperature to 800 °C and a heating rate of 10 K/min under N_2. X-ray diffraction (XRD) measurement was performed on a Rigaku D/MAX-rA diffractometer with Cu Kα radiation ($\lambda = 1.5406$ Å). N_2 adsorption experiments and micropore analysis were conducted at −196 °C using an Autosorb-1 from Quantachrome Instruments. Before adsorption measurements, the samples were degassed in vacuum overnight at 150 °C. CV-AAS was performed on an F732-S instrument (Shanghai Huaguang Machinery and Instrument Company, China). ICP-OES was conducted on a Vista MPX Simultaneous ICP-OES analyzer. ^{13}C cross-polarization magic-angle spinning (CPMAS) NMR spectra were recorded on a Varian InfinityPlus-400NMR spectrometer equipped with a standard Chemagnetic magic-angle spinning probe head, operating at 400.13 MHz for ^{1}H and 100.25 MHz for ^{13}C, respectively. Typically, about 50 mg sample was packed into a 4 mm zirconium oxide rotor and spun at about 10 kHz (±1 Hz). For the CPMAS NMR, the Hartmann-Hahn matching condition was optimized using hexamethylbenzene (HMB). Contact times were employed as 2 ms with the recycle delay of 2 s and proton 90° pulse length of 4.3 μs.

3. Results

3.1. Synthesis of SNW

To achieve MA-based porous polymers with high N content more efficiently, MA and TA have been used as monomers to synthesize the SNW in a catalyst-free process under microwaves through Schiff base chemistry. The synthetic route is outlined in Scheme 1. It forms a clear solution at the beginning of the reaction and then produces a great deal of precipitates quickly, affording off-white powders as products. At the same reaction conditions, the polymerization yield in this study (up to 90%, SNW-A, aldehyde is excessive) is much higher than that of conventional synthesis method [16]. Notably, non-reacted $-NH_2$ groups of the MA units can react with formaldehyde provided by the microwave-assisted thermal decomposition of DMSO to form methylol groups. Subsequently, these methylol groups can cross-link and two principle linkages are possible during condensation, namely an ether linkage or a methylene linkage, analogous to the cases observed from MA resin (Scheme 2) [32–34]. Hence, it shows that three principle linkages, including methine (–NH–CH–NH–) linkage, are formed at lower TA/MA ratio. However, this contribution to the synthesis of SNW at higher TA/MA ratio, if any, is very limited because the TA is excessive. Actually, heating this solvent with the aid of various catalysts is now an efficient alternative for the use of formaldehyde in many cases [19,20].

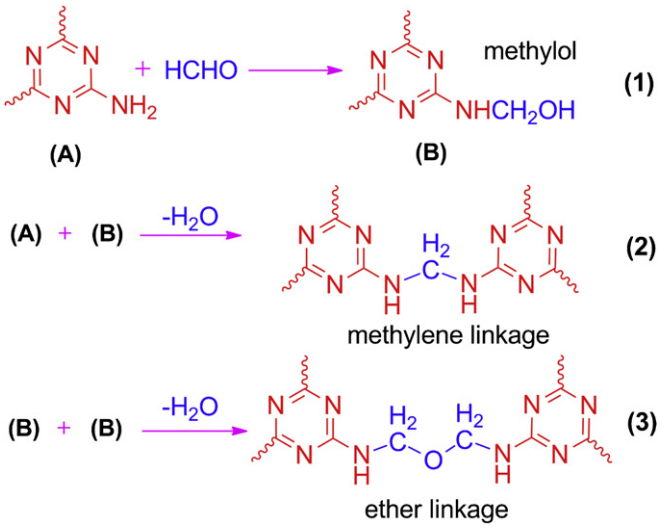

Scheme 2. A possible formation mechanism of methylene and ether linkages.

3.2. Structure analysis of SNW

The elemental analysis (C, H, N and S) of the different SNW samples is listed in Table 1. It can be seen that the nitrogen content gradually increases from 39 to 52 wt% with declining the TA/MA ratio from 2: 3 to 1: 7. Notably, the result also reveals a C/N atomic ratio of 1.398 for SNW-A; this ratio gradually decreases with increasing amount of MA, from 1.335 to 0.740 for SNW-B and SNW-G, respectively, which implies that changing with monomer ratios leads to a different polymer structure. To verify the proposed structure in Scheme 1, we acquired FT-IR, ^{13}C NMR, Raman, and XPS spectra analysis.

The FT-IR spectra of the monomers and the SNW with different monomer molar ratios are given in Fig. S1 (Supporting Information). As shown in Fig. S1a, the characteristic bands at 3419 and 3470 cm^{-1} ($-NH_2$ stretching) and 1650 cm^{-1} ($-NH_2$ deformation) on the spectrum of MA represent the three $-NH_2$ groups; and bands at 2870 (C–H stretching) and 1690 cm^{-1} (C=O stretching) on the spectrum of TA are attributable to the carbonyl function of the aldehydes (–CHO). The absence or sharp decrease in the intensity of these bands is an indication of a successful dehydration condensation reaction between the –CHO and $-NH_2$ groups. As seen in Fig. S1b, the appearance of a broad and strong band at around 3400 cm^{-1} (characteristic stretching of free N–H) in all samples, in addition to a band at 1150 cm^{-1} owing to the C–N stretching of secondary amine (–NH–), suggests a large number of –NH– and $-NH_2$ groups in all the SNW polymers [31]. But minor free hydroxyl groups and physisorbed water can also not be excluded to be responsible for the band at 3400 cm^{-1}. The distinct bands at 1563 and 1480 cm^{-1} (C=N vibrations of the s-triazine ring) confirm the successful incorporation of triazine units into the networks. Additionally, the absence of bands at 1613–1640 cm^{-1} (C=N stretching of azomethine) [35–37] indicates that aromatic aldimine (Ar–C=N–) does not exist on the surface of all the SNW polymers.

Because of the poor solubility of SNW polymers in common solvents, solid-state ^{13}C CPMAS NMR is further utilized to characterize the molecular structure (Fig. S2, Supporting Information). It further confirms the absence of imine bonds on the surface of SNW with no C=N resonance at 160 ppm [36,37]. The strong resonance at 167 ppm corresponds to the aromatic carbons of the triazine ring. The resonance peaks in the region of 120–142 ppm are correlated to aromatic carbons of the benzene ring. The 40–70 ppm region divides into two parts: (i) 60–70 ppm corresponding to carbon atoms present in methoxy functions and (ii) 40–60 ppm corresponding to carbon atoms in aminal units [33,38,39]. So we asserted that an aminal-linked network instead of an imine-linked

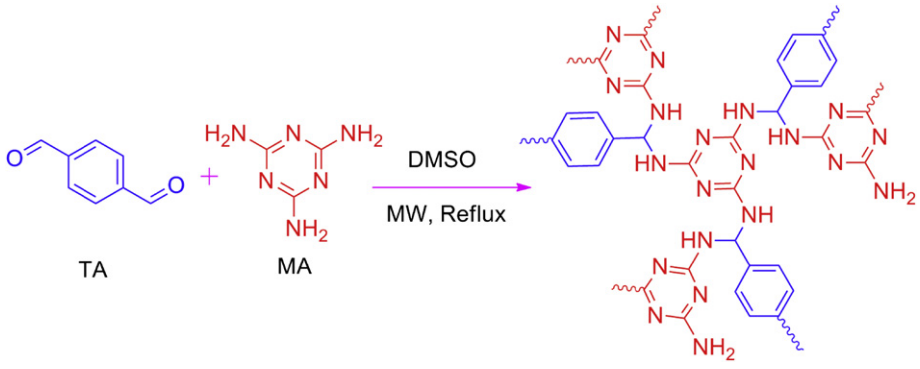

Scheme 1. The synthesis route used to prepare SNW polymers.

Table 1
Chemical elemental analysis of the SNW polymers resulting from different TA/MA molar ratios (180 °C, 4 h).

Samples	TA/MA[a]	Element analysis				
		C [wt%]	H [wt%]	N [wt%]	S [wt%]	C/N[b]
SNW-A	3:2	46.46	4.50	38.76	3.34	1.398
SNW-B	3:4	45.50	4.42	39.76	3.73	1.335
SNW-C	3:5	46.25	4.51	41.45	3.14	1.302
SNW-D	1:2	44.45	4.47	46.23	3.81	1.122
SNW-E	1:3	35.97	4.73	39.13	3.26	1.072
SNW-F	1:4	37.43	4.59	48.68	2.17	0.897
SNW-G	1:7	33.20	4.70	52.37	4.01	0.740

[a] Monomer molar ratio.
[b] Atomic ratio.

network is generated exclusively, in good agreement with literature data concerning the aminal [16,35,40]. A weak carbonyl peak is also observed at 194 ppm, attributed to unreacted aldehyde groups.

Raman spectroscopy has been well recognized as a very powerful technique for chemical and structural identification of MA and MA-based resins [34,41]. It is also applied to further analyse the molecular structure of the SNW (Fig. 1). Noticeable differences between the Raman (as well as FT-IR) spectra of the monomers and SNW samples indicate that the polymerization products are real polymers containing the two-monomer units rather than a simple complex or mixture of both monomers. The prominent peak at 676 cm^{-1} (deformation of the triazine ring) which is the characteristic peak of MA has been widely used as a marker to detect the existence of free MA in the foods or materials [41,42]. The disappearance of this peak could signify that there is no residual MA in the SNW samples or its content is below the Raman detection limit. Obviously, there is no trace of a band at 1650–1630 cm^{-1} (characteristic band of Ar–C=N–), which proves once again that the imine groups does not exist on the surface of all SNW polymers [35,43]. On the other hand, the band at 889 cm^{-1} can be ascribed to the C–N–C symmetric stretching of –NH– groups [43]. The other two feeble bands at 1170 and 1690 cm^{-1} can be described to benzene ring skeleton vibration and C=O stretching, respectively. All these apparent spectral changes agree with the formation of aminal links between the MA and TA, and further illustrate the effective cross-linking in the SNW polymers. The band intensities at 1609 and 1170 cm^{-1} (characteristic bands of benzene units), which are strongly related with the cross-linking level of polymer, increase with raising the TA/MA ratio of the sample (Fig. 1b), proving a higher degree of benzene units in SNW.

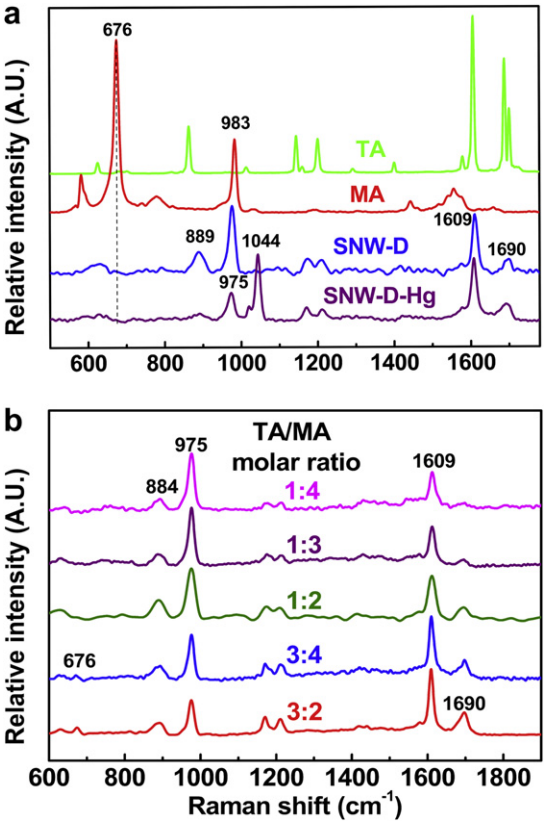

Fig. 1. (a) Raman spectra of the monomers, SNW-D and SNW-D-Hg (SNW-D equilibrated with 6 mM Hg^{2+} solution, pH = 2.3). (b) Raman spectra of SNW polymers resulting from different TA/MA ratios.

XPS data can nicely support the FT-IR, ^{13}C NMR and Raman data and reveal the surface binding states and elemental speciation of the SNW (Fig. 2). It is found that the SNW-D is comprised of C, N, O and S elements (Fig. 2a), and the mass content of these elements is given in Table 2. Peak fitting illustrates that C 1s of SNW-D (Fig. 2b) can be grouped into three peaks at 287.7, 284.9 and 286.7 eV corresponding to carbon atoms in triazine ring, benzene ring and the linkages (carbon atoms bonded to the more electronegative N or O atoms), respectively, indicating a successful crosslinking between the two monomers [32,44,45]. The N 1s peak at 398.8 eV (Fig. 2c) can be fitted into three peaks from the following groups: triazine groups (C=N–C) at 398.3 eV; –NH– groups at 399.8 eV; and $–NH_2$ groups at 399.2 eV [13,32,44,46]. The weak peak for O 1s is due to the minor O-containing groups (C–O–C, C–OH and C=O) as well as adsorbed water and carbon dioxide. A detailed analysis of the distribution of C and N species on SNW-D surfaces is shown in Table S2 (Supporting Information). Noteworthily, the elemental composition of SNW-D in the inner part and in the surface layer is analogous, as can be inferred from a comparison of the C/N atomic ratio determined by elemental analysis (1.122) and that calculated by XPS (1.179); which indicates that the functional groups in the samples are rather homogeneously distributed.

Another local structural technique that can provide information complementary to the above data is XRD analysis (Fig. S3, Supporting Information). All diffractograms exhibit three broad diffraction peaks at the Bragg angle of approximately 21° (strong), 12° (medium) and 41° (weak), which reveals that the SNW polymers are amorphous, quite different from the crystalline structure of both monomers. These peaks become stronger with decreasing the TA/MA ratio from 3: 2 to 1: 4, implying that the crystallinity increases as increasing the amount of MA. This behaviour is due to the high content of MA with more amine groups that are easy to form hydrogen bonds between the MA-based molecules.

To investigate the microstructure of the SNW polymers, several typical samples were characterized by SEM. The SEM image of SNW-A (Fig. 3a) reveals a series of agglomerates of interconnected imperfect-spherical nanoparticles confined within a continuous pore network. SNW-B is formed out of irregular, aggregated micro- and nanoparticles, and the porosity is mainly interstitial (Fig. 3b). Contrastingly, SNW-D is composed of various irregular-shaped microparticles, exhibiting an “eroded rock”-like surface with some macropores in it (Fig. 3c). These results lead to the conclusion that higher concentrations of MA in the sample yield larger sized particles. Moreover, these amorphous, irregular and loosely packed nanostructures that are important in enhancing the accessibility of adsorbates to reactive sites would be potential advantage in adsorption of metal ions [31].

The N_2 adsorption–desorption isotherms (Fig. S4, Supporting Information) were also used to elucidate the porous properties of the SNW, and the analysis results are summarized in Table 3. The adsorption isotherms show a steep gas uptake at low relative pressures, which represents the presence of microporosity in the

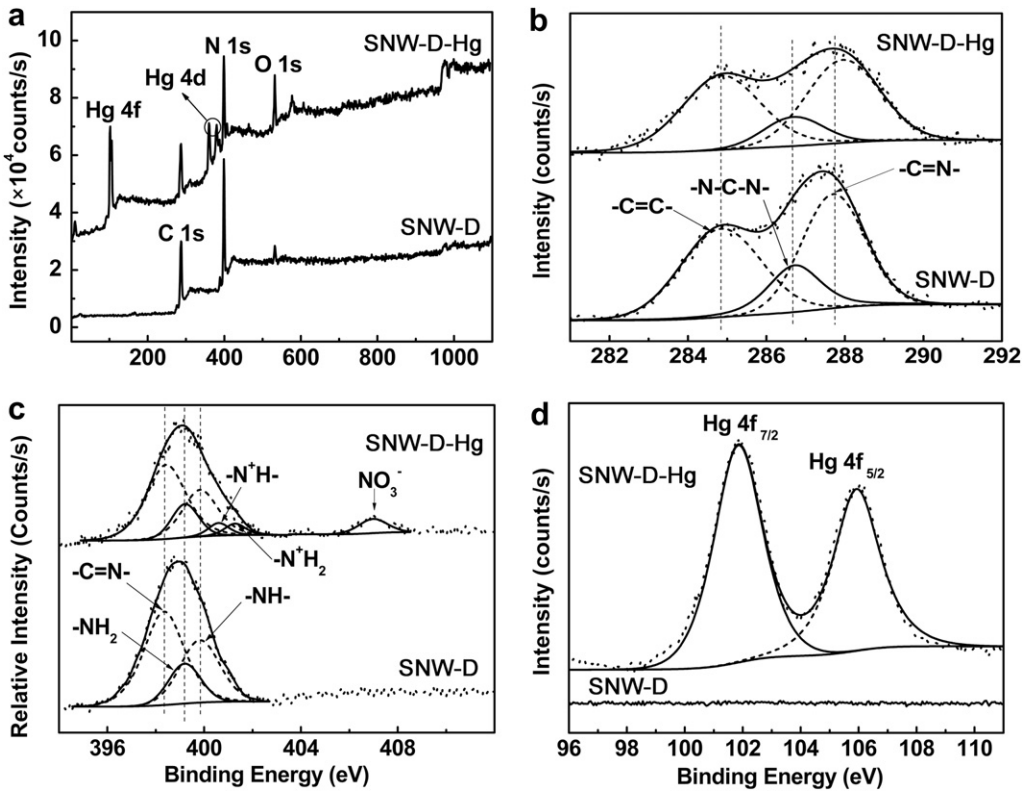

Fig. 2. XPS spectra of survey scan (a) and high-resolution scan of C 1s (b), N 1s (c) and Hg 4f (d) for SNW-D and SNW-D-Hg.

samples; and Horvarth-Kawazoe pore size distribution (Fig. S5, Supporting Information) indicates that the micropore size is mainly less than 1 nm. But the broad pore size distribution calculated from Barrett-Joyner-Haladan (BJH) model demonstrates that all the networks lack uniform pore structures (data not shown). The BJH average pore diameter is about 14 nm, pointing to lots of meso- and macroporous structures in the samples. As expected, decreasing TA/MA ratio from 2: 3 to 1: 4 results in a substantial decrease of specific surface area from 301 to 133 $m^2\ g^{-1}$, together with the pore volume from 0.30 to 0.11 $cm^3\ g^{-1}$ (Table 3), which might be speculated as a result of more relative hydrogen bonds in the high MA content networks. It can also be inferred that the introduction of benzene spacer groups into the networks can effectively enhance the porosity and surface area. Therefore, the morphology and the surface area can be well tuned by varying the molar ratios. It is noticeable that these values of surface area are comparable to or greater than the recently described porous MA resins prepared by soft templating [33], microemulsion [47] and silica templating [44]. However, the specific surface area of SNW in this work is much lower than those reported by Schwab et al. [16] Though the microwave irradiation can boost the yield and speed of the reaction, the reaction time in this paper is only 4 h which is much shorter than 72 h in previous report. So the most likely reason for the lower specific surface area is that the SNW in this paper possess lower degree of crosslinking, and thus affords more amine-terminated groups than that reported. And these amine groups are easy to form hydrogen bonds between the MA-based molecules, leading to the decrease in porosity as well as specific surface area.

Table 2
Elemental binding energy and mass content of SNW-D before and after Hg sorption.

	N 1s	C 1s	S 2p	O 1s	Hg 4f
SNW-D [eV]	398.82	286.45	164.36	531.6	
SNW-D-Hg [eV]	399.19	286.33	165.65	532.4	101.88
SNW-D [wt%]	44.73	45.21	3.64	6.42	
SNW-D-Hg [wt%]	23.43	24.50	1.47	9.00	41.61

3.3. Properties of SNW

3.3.1. Solubility

The SNW polymers are totally insoluble in all organic solvents tested, H_2O, and alkaline solution, however, showing limited solubility in inorganic strong acid solution (Table S1, Supporting Information). They are all soluble in concentrated H_2SO_4 and form a brown solution and exhibit gradually enhanced solubility in HNO_3 (3 M) and H_2SO_4 (3 M) with raising MA content in the sample, probably due to higher MA content of SNW with more free amino groups that can interact with hydrogen ion. These observations prove that the materials can resist alkaline, acidic, and solvents media, and largely maintain the original structure. Hence, the SNW particles are allowed to be used as adsorbent or catalyst support in complicated environment.

3.3.2. Thermal stability

TGA curves of the SNW polymers as well as monomers are displayed in Fig. S6 (Supporting Information). The pure MA and TA only shows one sharp mass loss at 310 and 160 °C, respectively, which are significantly different from the SNW, proving once again that the polymerization products are indeed genuine polymers rather than a simple mixture of two monomers. The SNW polymers exhibit a smaller weight-loss process before 300 °C, and then a single major decomposition starting at a temperature above 400 °C. The first gradual mass loss can be related to out-gassing of carbon dioxide, moisture and solvent trapped inside the polymers. But the dehydration reaction between the minor methylol groups upon heating can also contribute to this process. The second step in

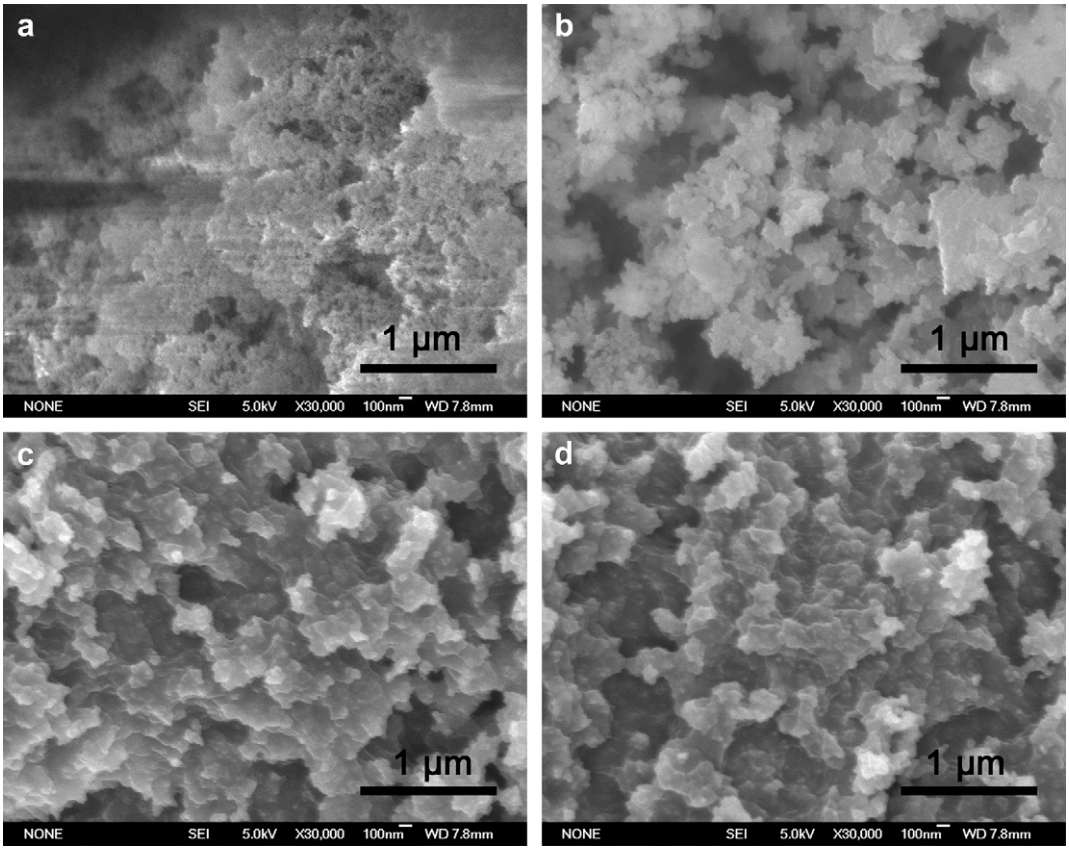

Fig. 3. SEM images of SNW-A (a), SNW-B (b), SNW-D (c) and SNW-D-Hg (d).

the TGA curve can be explained by the thermal degradation of MA units or other advanced condensates. And this process of thermal decomposition may be accompanied by a post-polycondensation process, where the polymer $-NH_2$ and $-CHO$ end groups continue to react and water is expelled [48].

3.3.3. Photoluminescence (PL)

We also studied the PL properties of the SNW polymers. PL spectra were recorded with an excitation wavelength of 386 nm (Fig. S7, Supporting Information). The maximum emission wavelength is 457 nm when dispersed in some solvents (e.g., H_2O, DMF, acetone, EtOH, THF and CH_2Cl_2). However, it produces green luminescence with emission band at 494 nm when dispersed in DMSO. Noteworthily, the PL properties of all these polymers are similar, and the emission colors are all close to blue. The blue-white fluorescence of the solid samples can also be seen under UV light (365 nm) by naked eyes (Fig. S8d, Supporting Information). Interestingly, the filtrate of the final products can also produce similar fluorescence in different solvents (Fig. S8a–b, Supporting Information), maybe owing to some polymers with low degree of crosslinking are still soluble in the filtrate after the reaction. It is generally accepted in the literature that N incorporation plays a key role in PL emission [49–51]; and that the PL properties of SNW may correlate with the s-triazine units, which are in close resemblance to that of carbon nitride [50] and polyamine [52].

Table 3
Pore characteristics of the SNW polymers.

Samples	S_{BET} [$m^2\ g^{-1}$] [a]	V_{total} [$cm^3\ g^{-1}$] [b]	V_{micro} [$cm^3\ g^{-1}$] [c]	d_p [nm] [d]
SNW-A	301	0.30	0.114	14.1
SNW-B	219	0.22	0.084	14.0
SNW-D	153	0.15	0.056	14.3
SNW-E	115	0.11	0.043	13.9

[a] BET surface area.
[b] Pore volume calculated from nitrogen adsorption at $p/p^0 = 0.8$.
[c] Micropore volume calculated from nitrogen adsorption at $p/p^0 = 0.1$.
[d] BJH average pore diameter calculated from desorption data.

3.4. Adsorption of Hg on SNW particles

3.4.1. Optimization of the TA/MA ratio for Hg^{2+} adsorption

As shown in Fig. 4, the Hg^{2+} adsorption capacity and adsorptivity on the SNW particles increase first and then decrease with increasing MA content. Particularly, the SNW-C particles with MA feed content of 62.5 mol% possess the maximal adsorption capacity and adsorptivity up to 543 mg g^{-1} and 90.4%, respectively. The enhancement of adsorbability with increasing MA content from 40 to 62.5 mol% may be attributed to more MA molecules being polymerized into the SNW polymers, affording more binding sites for Hg^{2+} on the surface. It is therefore reasonable to assume that the coordination interaction of N atoms and Hg^{2+} is an important factor for the superior adsorption performance. Yet when the MA content exceeds 62.5 mol%, the adsorbability decreases remarkably with increasing MA content, which may be attributed to the decline of the specific surface area (see Table 3). The low specific surface area will allow limited surface sites for Hg^{2+}, in accordance with literature [53]. In other words, both the specific surface area value and N content can influence the adsorption of Hg^{2+}; and the optimal combination is at the 62.5 mol%. However, increasing the amount of MA can reduce costs because TA monomer is more expensive than MA. Consequently, the SNW-D with MA feed content of 66.7 mol%, also exhibiting a high Hg^{2+} adsorbance (527 mg g^{-1}), will be optimum for further Hg^{2+} adsorption.

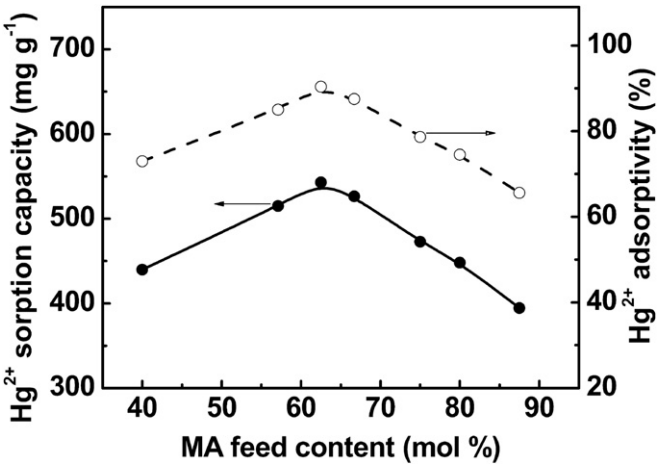

Fig. 4. Variation of adsorption capacity and adsorptivity of Hg^{2+} onto SNW particles with MA feed content at initial Hg^{2+} concentration of 6 mM in $Hg(NO_3)_2$ solution for 24 h.

3.4.2. Adsorption kinetics

The speed of adsorption of Hg^{2+} on SNW-D at initial concentration of 2 mM and 10 mM is presented in Fig. 5. In 2 mM Hg^{2+} solution (Fig. 5a), instantaneous adsorption occurs within 2 min, for which the adsorption capacity and adsorptivity reach up to 175 mg g^{-1} and 87.5%, respectively. But the adsorption becomes slow from 10 to 1500 min and more than 98% of Hg^{2+} is removed after 1440 min (24 h). In 10 mM Hg^{2+} solution (Fig. 5b), 64% of Hg^{2+} is adsorbed within 30 min, and more than 80% of Hg^{2+} is removed after 24 h. It attains equilibrium with the adsorption capacity of 841 mg g^{-1} and adsorptivity of 84% at the adsorption time of 48 h. Thus, the adsorption rate is much faster at lower Hg^{2+} concentration than at higher concentration. Apparently, high adsorption rates are observed at the beginning of adsorption process (ca. < 10 min), followed by a slow uptake (ca. 1–2 days) in both 2 mM and 10 mM Hg solution. The rapid adsorption at the beginning is considered to be the consequence of its unique properties of surface morphology and the fast interaction between Hg^{2+} and abundant N-containing groups on the surface, while the slow uptake can be due to multisorption sites with different adsorption kinetics or due to slow conversion from outer- to inner-sphere surface complexes [21,54]. These results are much faster than some commonly used Hg^{2+} sorbents [21,55–57], which require more time for 90% adsorption of Hg^{2+}. This unique character could make the SNW polymer sorbents suitable for solid phase extraction or other applications that require fast adsorption of Hg^{2+}.

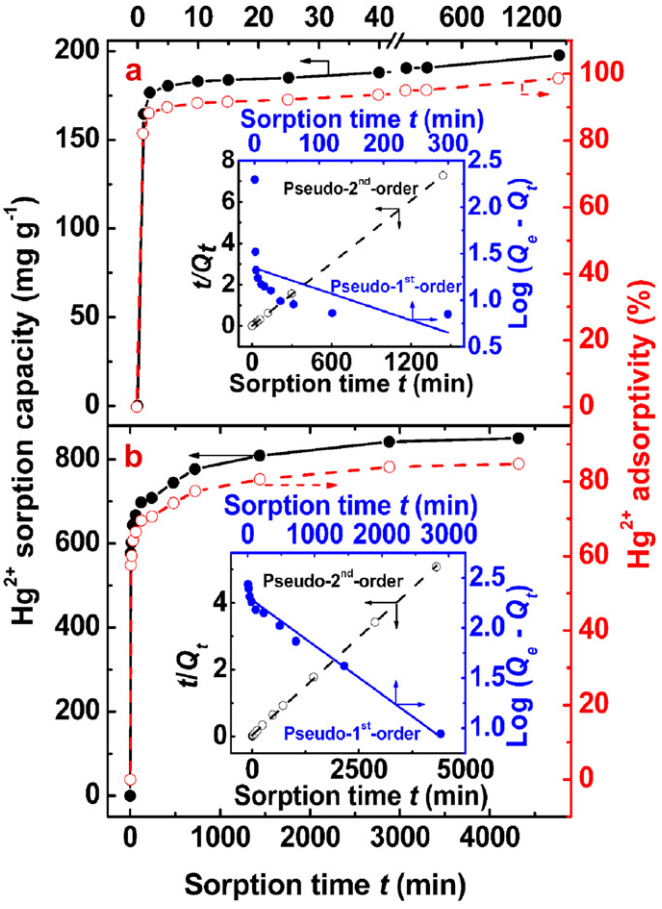

Fig. 5. Effect of adsorption time on Hg^{2+} adsorption onto SNW-D, at initial Hg concentrations of 2 (a) and 10 mM (b) in $Hg(NO_3)_2$ solution. Inset: The pseudo-first-order and pseudo-second-order plots of the adsorption data.

In order to assess the kinetic mechanism that controls the adsorption process, pseudo-first-order and pseudo-second-order models were used [58]. The fitting results and kinetic parameters are presented in Fig. 5 (inset) and Table 4, respectively. Based on the obtained correlation coefficients, the pseudo-second-order equation is the model that furthered the best fit for the experimental kinetic data, suggesting the Hg^{2+} adsorption on SNW-D may be a chemical process involving valence forces through sharing or exchange of electrons between adsorbent and sorbate [58,59].

3.4.3. Adsorption isotherm

Adsorption isotherms can predict the adsorption efficiency and potential of an adsorbent. For this reason, the adsorption isotherms of Hg^{2+} for SNW were investigated (Fig. 6). At lower initial Hg^{2+} concentrations, especially in the range of 0–10 mM, it can be seen clearly that the adsorption capacity of Hg ions rises significantly with increasing initial concentrations, whereas the adsorptivity declines. Finally at higher concentrations, the increase of adsorption capacity becomes very slow because the adsorption process approaches saturation of the active binding sites gradually. The highest adsorptivity achieved in this study is 98.9% at initial Hg^{2+} concentration of 1 mM. That is to say, almost all Hg^{2+} will be adsorbed onto the SNW-D if the initial Hg^{2+} concentration is lower than 1 mM.

To estimate the best fitting model to the experimental data, isotherms were modeled according to the Freundlich and Langmuir equilibrium models [31]. It is evident from Fig. 6 (inset) and Table 4 that a more precise fit of isotherm data is shown by Langmuir model, as in virtue of higher correlation coefficient than by Freundlich model, implying that the Hg^{2+} adsorption on SNW-D may be a monolayer adsorption. The maximum theoretical adsorption capacities of Hg on SNW-D calculated from Langmuir equation is 1165 mg g^{-1}, slightly lower than the experimental maximum adsorbance of 1172 mg g^{-1}. In addition, this adsorbance of SNW-D is comparable to or better than other polymer sorbents, which were widely described in the literatures [21,27,57,58].

3.4.4. Selective adsorption

To evaluate the selectivity of the SNW-D, competitive adsorption of Hg^{2+} with other interfering cations, such as Cu^{2+}, Cd^{2+}, Ni^{2+}, Zn^{2+}, Co^{2+}, Ca^{2+}, Mn^{2+}, and Mg^{2+} was performed. In this set of experiments, the initial concentration of each ion in the mixed solution was fixed at 20 ppm. Fig. 7 displays the uptake of heavy metal ions after 30 min contact time. It can be seen that only Hg^{2+} is effectively removed by SNW-D(98.5%), while less than 5% of Ca^{2+},

Table 4
Kinetics and isotherm model equations for Hg^{2+} adsorption onto SNW-D based on the data in Figs. 5 and 6.

Mathematical model	Hg^{2+} [mM]	Equation	Correlation coefficient	Q_e , Q_m [mg g^{-1}] or n	k'[min^{-1}], h [mg g^{-1} min^{-1}], K_a [L mg^{-1}] or K_F
Pseudo-1st-order	2	Log $(Q_e - Q_t) = -0.00231t + 1.3445$	0.1730	$Q_e = 199$	$k' = 0.005320$
	10	Log $(Qe - Qt) = -0.000486t + 2.3119$	0.9864	$Q_e = 851$	$k' = 0.001119$
Pseudo-2nd-order	2	$t/Q_t = 0.005060t + 0.01181$	0.9999	$Q_e = 198$	$h = 84.67$
	10	$t/Q_t = 0.001174t + 0.03945$	0.9998	$Q_e = 852$	$h = 25.35$
Langmuir	–	$C_e/Q_e = 0.0008583C_e + 0.1065$	0.9974	$Q_m = 1165$	$K_a = 0.00806$
Freundlich	–	Log $Q_e = 0.2580$ log $C_e + 2.1362$	0.8349	$n = 3.877$	$K_F = 136.8$

Mn^{2+} and Mg^{2+} ions are removed. About 15% of Cu^{2+}, 13% of Cd^{2+}, 8% of Ni^{2+} and Co^{2+} and 7% of Zn^{2+} are adsorbed by SNW. It proves that the SNW-D can very selectively and effectively scavenge Hg from wastewater, allowing the selective extraction of Hg^{2+} from complex mixtures. However, SNW-D cannot be expected to be a specific adsorbent for Hg^{2+}, because the electron donor is N atom. This unexpected result may be attributed to an additional complexation by the S-containing groups derived from the rapid microwave-assisted decomposition of the DMSO [19] or to a certain specific combination of N- and S-containing functional groups on the polymer networks.

4. Discussion

Though the MA and MA-based materials (i.e., MF and modified-MF organic resins) are filled with N lone-pair electrons which thought to be potentially ideal sites for metal complexes, surprisingly the coordination chemistry of these N ligands remains rarely explored. This is mainly believed to be the results of the strong rigidity of the N-heterocycle and the trend to form hydrogen bonds between MA-based molecules [60]. So the observed strong adsorption capability in the removal of Hg^{2+} on SNW polymers, here, is an astonishing phenomenon, and it may be due to the following factors: (i) the introduction of distinctive benzene spacer groups, which may reduce the hydrogen bonds and hence activate the numerous amine as well as triazine groups; (ii) the doping of S-containing ligands that can strongly interact with Hg; (iii) the special surface morphology and amorphous nanostructures with intrinsic microporosity, which is very beneficial for adsorption of heavy metal ions [61].

To identify the possible adsorption sites of Hg^{2+} ions bonded to the SNW, FT-IR, Raman and XPS spectra were obtained for SNW-D before and after the Hg^{2+} adsorption. From the FT-IR spectra of SNW-D-Hg (Fig. S1a, Supporting Information), it can be seen that the band at 3400 cm^{-1} red-shift to 3368 cm^{-1} and bands at 1565 and 1480 cm^{-1} get broader and red-shift to 1560 and 1460 cm^{-1}, respectively. In the Raman spectra (Fig. 1a), bands which can be assigned to C—N stretching (889 cm^{-1}) of the —NH— groups as well as to the ring breathing of the triazine ring (975 cm^{-1}) are strongly attenuated in the spectra of the SNW-D-Hg. These changes are most probably caused by forming complex between SNW-D and Hg, with more electrons delocalized extensively among vacant d orbit of Hg and p orbit of N atoms [62]. Moreover, it is likely that all the N-containing functional groups on the polymer matrix including triazine ring, $-NH_2$ and —NH— groups could take part in the complexation. The sharply peak at 1043 cm^{-1} in Raman spectra as well as the new strong sharp absorption peak of 1380 cm^{-1} in FT-IR spectra of SNW-D-Hg is identified to be nitrates (NO_3^-), remaining as charge-balancing anion in the complex [28]. It should be note that the initial pH of Hg^{2+} solutions in the adsorption experiments is lower than 3 and thus the dominant Hg species is Hg^{2+}. Therefore, these observations agree with the formation of charged complexes, according to the reports in the literature [28,63].

Strong Hg signals detected from the XPS survey spectrum of the SNW-D-Hg (Fig. 2a) clearly confirm the adsorption of Hg, agreeing well with the TGA results (Fig. S9, Supporting Information). The binding energy of N 1s and S 2p on the SNW-D-Hg surface increases slightly as compared with those on SNW (Table 2), which illuminates that N and S atoms are electron donors during the Hg adsorption and that the Hg adsorption on the SNW surface is likely accomplished through the chemical coordination of Hg ions with N and S atoms in the surface functional groups [23,64,65]. On the other hand, with the appearance of Hg 4f and Hg 4d peaks after Hg^{2+} adsorption, the intensity of the N 1s peak is decreased significantly, suggesting the strong interaction between Hg^{2+} and N [22]. As depicted in Fig. 2c, N 1s of SNW-D-Hg contains three more new peaks than SNW at 407.0, 400.6, and 401.3 eV, which are linked

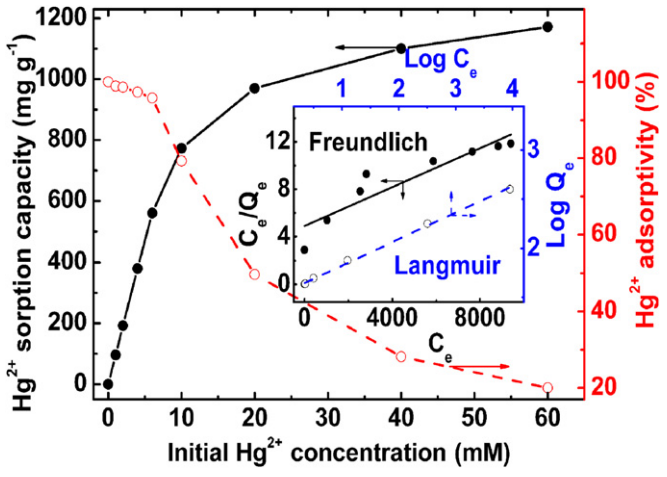

Fig. 6. Effect of initial Hg^{2+} concentration on adsorption of Hg^{2+} on SNW-D particles in $Hg(NO_3)_2$ solution for 24 h. Inset: Langmuir and Freundlich plots of the adsorption data in the concentrations range from 0.5 to 60 mM.

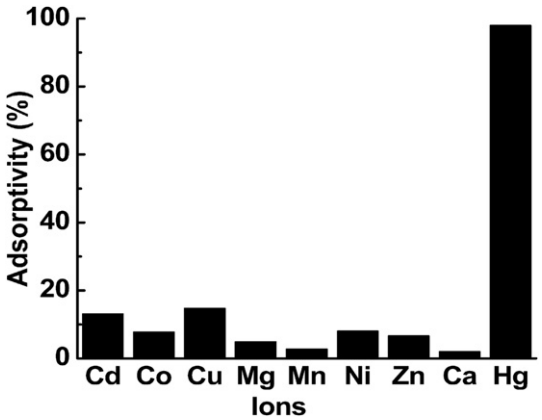

Fig. 7. Selectivity of the SNW-D adsorbent for Hg^{2+} in the mixture of different divalent ions solution; Initial concentration of each ion: 20 ppm; pH = 4.2.

to NO_3^-, protonated $-N^+H_2$ and $-N^+H-$ groups, respectively (for details, Table S2, Supporting Information). Accordingly, the increase of the O1s peak at about 532.4 eV after adsorption can mainly be attributed to the NO_3^-. The Hg 4f region (Fig. 2d) is comprised of two peaks at 101.8 (Hg $4f_{7/2}$) and 105.9 eV (Hg $4f_{5/2}$), with a spin-orbit splitting of 4.1 eV. The absence of Hg $4f_{7/2}$ peaks lower than 100.6 eV, indicates that Hg^0 (binding energy around 99.8 eV) is not present at the SNW-D surface [64,65]. Although the concentration of S-containing ligands is low (2–4 wt% of S) for SNW, they may also play a hugely important role in the Hg adsorption. For example, the humic acid that contains low concentration of S-containing ligands has been ascribed as the main binding sites in view of their extremely high affinity toward Hg^{2+} [22,66]. Consequently, it can be concluded that both the N- and S-containing groups could be responsible for the Hg adsorption.

Few Hg^+ can only be detected at high initial concentrations (>10 mM) after long enough contact time (>8 h) by NaCl test method [21], implying that the redox adsorption of SNW-D in this paper is almost negligible. On the basis of this study, a schematic mechanism for Hg uptake by SNW is proposed (see the Graphical Abstract). The dominant mechanism of the interaction is due to the presence of free lone pairs of electrons on N and S atoms that are suitable for coordination with Hg to give the corresponding SNW–Hg complex. More studies, however, are needed to further understand the mechanism for Hg^{2+} adsorption as well as selective adsorption, and expand the applications of SNW polymers.

Through analyzing the SEM images of the SNW-D before and after Hg^{2+} adsorption (Fig. 3c and d), we found that no discernible difference is observable; which implies that the adsorbed Hg^{2+} may be uniformly distributed on the surface of SNW-D. On the other hand, the peaks assigned to the triazine and benzene ring skeleton structure in the FT-IR and Raman spectra hardly change during Hg^{2+} adsorption in acidic solution, and this indicates that no structure changes occur in the polymer backbone.

5. Conclusions

In summary, we take advantage of high efficiency of the microwave irradiation to prepare highly cross-linked porous aminal networks through Schiff base chemistry. The as-prepared SNW polymers possess several unique characteristics: the facile one-pot synthesis; cheap and simple monomers; high N content (up to 50 wt%); in situ doped with S; high yield (up to 90%); catalyst-free; solvent-dependent fluorescence property and high chemo-resistance (thermal and chemical stability). Compared with previous method, this strategy is more efficient, convenient, and time saving and can be extended to large-scale fabrication. Hg adsorption tests demonstrate that, for the first time, the SNW polymers can very effectively and selectively scavenge Hg^{2+} from strong acidic waters without destroying the host structure. All these advantages substantially make these materials promising candidates for potential applications in catalysis, separation, solid-phase extraction, Hg elimination, and sensing. More importantly, we found that the incorporation of distinctive benzene spacer groups into the polymer networks can deeply influence the polymer properties and characteristics. And knowledge on the structural aspects as well as adsorption mechanisms would potentially facilitate unearthing novel materials or technologies for effective and selective removal of Hg^{2+} from wastewater.

Acknowledgment

The authors gratefully acknowledge the support for this research by National Natural Science Foundation of China (20975042), the Program for Academic Pacesetter of Wuhan (200851430484), Nature Science Foundation Key Project from Hubei Province of China (2008CDA080) and International Science and Technology Cooperation and Exchange Foundation (2008DFA40270).

Appendix. Supporting information

Supplementary data related to this article can be found online at doi:10.1016/j.polymer.2010.10.052

References

[1] McKeown NB, Budd PM. Chem Soc Rev 2006;35:675–83.
[2] Germain J, Fréchet JMJ, Svec F. Small 2009;5:1098–111.
[3] Zhang Y, Wei S, Liu F, Du Y, Liu S, Ji Y, et al. Nano Today 2009;4:135–42.
[4] El-Kaderi HM, Hunt JR, Mendoza-Cortes JL, Cote AP, Taylor RE, O'Keeffe M, et al. Science 2007;316:268–72.
[5] Jiang J-X, Cooper A. Microporous organic polymers: design, synthesis, and function. Berlin: Springer; 2010. 1–33.
[6] McKeown NB, Budd PM. Macromolecules 2010;43:5163–76.
[7] Kuhn P, Antonietti M, Thomas A. Angew Chem Int Ed 2008;47:3450–3.
[8] Mooibroek TJ, Gamez P. Inorg Chim Acta 2007;360:381–404.
[9] Steffensen MB, Hollink E, Kuschel F, Bauer M, Simanek EE. J Poly Sci Part A Poly Chem 2006;44:3411–33.
[10] Jurgens B, Irran E, Senker J, Kroll P, Muller H, Schnick W. J Am Chem Soc 2003;125:10288–300.
[11] Hulicova D, Yamashita J, Soneda Y, Hatori H, Kodama M. Chem Mater 2005;17:1241–7.
[12] Wang X, Maeda K, Thomas A, Takanabe K, Xin G, Carlsson JM, et al. Nat Mater 2009;8:76–80.
[13] Pevida C, Drage TC, Snape CE. Carbon 2008;46:1464–74.
[14] Kuhn P, Al Forget, Su D, Thomas A, Antonietti M. J Am Chem Soc 2008;130:13333–7.
[15] Chan-Thaw CE, Villa A, Katekomol P, Su D, Thomas A, Prati L. Nano Lett 2010;10:537–41.
[16] Schwab MG, Fassbender B, Spiess HW, Thomas A, Feng X, Müllen K. J Am Chem Soc 2009;131:7216–7.
[17] Kappe C, Dallinger D. Mol Divers 2009;13:71–193.
[18] Bilecka I, Niederberger M. Nanoscale 2010;2:1358–74.
[19] Mésangeau C, Yous S, Pérès B, Lesieur D, Besson T. Tetrahedron Lett 2005;46:2465–8.
[20] Cao A, Liu Z, Chu S, Wu M, Ye Z, Cai Z, et al. Adv Mater 2009;22:103–6.
[21] Li X-G, Feng H, Huang M-R. Chem Eur J 2009;15:4573–81.
[22] Wang J, Deng B, Chen H, Wang X, Zheng J. Environ Sci Technol 2009;43:5223–8.
[23] Zhu J, Deng B, Yang J, Gang D. Carbon 2009;47:2014–25.
[24] Xiao B, Thomas KM. Langmuir 2005;21:3892–902.
[25] Bell CA, Smith SV, Whittaker MR, Whittaker AK, Gahan LR, Monteiro MJ. Adv Mater 2006;18:582–6.
[26] Sinner F, Buchmeiser MR, Tessadri R, Mupa M, Wurst K, Bonn GK. J Am Chem Soc 1998;120:2790–7.
[27] Bessbousse H, Rhlalou T, Verchére J-Fo, Lebrun L. J Phys Chem B 2009;113:8588–98.
[28] Billinge SJL, McKimmy EJ, Shatnawi M, Kim H, Petkov V, Wermeille D, et al. J Am Chem Soc 2005;127:8492–8.
[29] Liu X, Qi C, Bing T, Cheng X, Shangguan D. Talanta 2009;78:253–8.
[30] Li X-G, Dou Q, Huang M-R. Monatsh Chem 2008;139:1157–62.
[31] Li X-G, Liu R, Huang M-R. Chem Mater 2005;17:5411–9.
[32] Coullerez G, Léonard D, Lundmark S, Mathieu HJ. Surf Interface Anal 2000;29:431–43.
[33] Kailasam K, Jun Y-S, Katekomol P, Epping JD, Hong WH, Thomas A. Chem Mater 2009;22:428–34.
[34] Meier RJ, Tiller A, Vanhommerig SAM. J Phys Chem 1995;99:5457–64.
[35] Layer RW. Chem Rev 1963;63:489–510.
[36] Kaya I, YildIrIm M. Synth Met 2009;159:1572–82.
[37] Pandey P, Katsoulidis AP, Eryazici I, Wu Y, Kanatzidis MG, Nguyen ST. Chem Mater 2010;22:4974–9.
[38] Egger CC, Schädler V, Hirschinger J, Raya J, Bechinger B. Macromol Chem Phys 2007;208:2204–14.
[39] Baraka A, Hall PJ, Heslop MJ. React Funct Polym 2007;67(7):585–600.
[40] Forlani LSM, Todesco PE. Gazz Chim Ital 1986;116:229–32.
[41] Liu Y, Chao K, Kim M, Tuschel D, Olkhovyk O, Priore R. Appl Spectrosc 2009;63:477–80.
[42] Scheepers ML, Meier RJ, Markwort L, Gelan JM, Vanderzande DJ, Kip BJ. Vib Spectrosc 1995;9:139–46.
[43] Socrates G. Infrared and Raman Characteristic Group Frequencies: Tables and Charts. 3rd ed. New York: Wiley; 2004.
[44] Deryło-Marczewska A, Goworek J, Pikus S, Kobylas E, Zgrajka W. Langmuir 2002;18:7538–43.
[45] Matsui T, Yudasaka M, Kikuchi R, Ohki Y, Yoshimura S. Appl Phys Lett 1994;65:2145–7.
[46] Li X-G, Ma X-L, Sun J, Huang M-R. Langmuir 2009;25(3):1675–84.

[47] du Fresne von Hohenesche C, Schmidt DF, Schädler V. Chem Mater 2008;20:6124–9.
[48] Hindson J, Ulgut B, Friend R, Greenham N, Norder B, Kotlewski A, et al. J Mater Chem 2010;20:937–44.
[49] Papadimitriou D, Roupakas G, Dimitriadis C, Logothetidis S. J Appl Phys 2002;92:870–5.
[50] Zhao Y, Liu Z, Chu W, Song L, Zhang Z, Yu D, et al. Adv Mater 2008;20:1777–81.
[51] Fei B, Yang Z, Shao S, Wan S, Xin JH. Polymer 2010;51:1845–52.
[52] Mahapatra SS, Karak N. Poly J 2009;41:20–5.
[53] Cai JH, Jia CQ. Ind Eng Chem Res 2010;49:2716–21.
[54] Jeon B-H, Dempsey BA, Burgos WD, Royer RA. Water Res 2003;37:4135–42.
[55] Xiong C, Yao C. Chem Eng J 2009;155:844–50.
[56] Zhang Y, Li Q, Sun L, Tang R, Zhai J. J Hazard Mater 2009;175:404–9.
[57] Li N, Bai R, Liu C. Langmuir 2005;21:11780–7.
[58] Inbaraj BS, Wang JS, Lu JF, Siao FY, Chen BH. Bioresour Technol 2009;100:200–7.
[59] Huang M-R, Peng Q-Y, Li X-G. Chem Eur J 2006;12:4341–50.
[60] Zhang L, Zhang J, Li Z-J, Cheng J-K, Yin P-X, Yao Y-G. Inorg Chem 2007;46:5838–40.
[61] Wang Y, Wang G, Wang H, Liang C, Cai W, Zhang L. Chem Eur J 2010;16:3497–503.
[62] Ma N, Yang Y, Chen S, Zhang Q. J Hazard Mater 2009;171:288–93.
[63] Tchinda Al J, Ngameni E, Kenfack IT, Walcarius A. Chem Mater 2009;21:4111–21.
[64] Hutson ND, Attwood BC, Scheckel KG. Environ Sci Technol 2007;41:1747–52.
[65] Bond AM, Miao W, Raston CL. Langmuir 2000;16:6004–12.
[66] Hesterberg D, Chou JW, Hutchison KJ, Sayers DE. Environ Sci Technol 2001;35:2741–5.